

---

---

# A Gelatin Liver Phantom of Suspended $^{90}\text{Y}$ Resin Microspheres to Simulate the Physiologic Microsphere Biodistribution of a Postradioembolization Liver

Yung Hsiang Kao<sup>1,2</sup>, Oliver S. Luddington<sup>1</sup>, Simone R. Culleton<sup>1</sup>, Roslyn J. Francis<sup>1,3</sup>, and Jan A. Boucek<sup>1</sup>

<sup>1</sup>Department of Nuclear Medicine, Sir Charles Gairdner Hospital, Perth, Western Australia, Australia; <sup>2</sup>Department of Nuclear Medicine, Austin Hospital, Melbourne, Victoria, Australia; and <sup>3</sup>School of Medicine and Pharmacology, University of Western Australia, Perth, Western Australia, Australia

---

For phantom studies involving  $^{90}\text{Y}$  PET/CT, homogeneous solutions of  $^{90}\text{Y}$ , for example,  $^{90}\text{Y}$  citrate, are commonly used. However, the microsphere biodistribution of a postradioembolization liver is never homogeneous; therefore, such phantoms are physiologically unrealistic for simulating clinical scenarios. The aim of this work was to develop a safe and practical phantom capable of simulating the heterogeneous microsphere biodistribution of a postradioembolization liver. **Methods:** Gelatin (5%) was used to suspend  $^{90}\text{Y}$  resin microspheres, poured into plastic containers to simulate a liver with 2 tumors. Microspheres were added while the gelatin was maintained in a liquid state on a hot plate and continuously stirred with magnetic stir bars. The liquid microsphere mixture was then rapidly cooled in an ice bath while being stirred, resulting in a heterogeneous suspension of microspheres. The completed phantom was serially scanned by  $^{90}\text{Y}$  PET/CT over 2 wk. **Results:** All scans demonstrated a heterogeneous microsphere distribution throughout the liver and tumor inserts. Serendipitously, magnetic stir bars left inside the phantom produced CT artifacts similar to those caused by embolization coils, whereas pockets of air trapped within the gelatin during its preparation mimicked gas within hollow viscus. The microspheres and tumor inserts remained fixed and suspended within the gelatin, with no evidence of breakdown or leakage. **Conclusion:** A gelatin phantom realistically simulating the physiologic microsphere biodistribution of a postradioembolization liver is feasible to construct in a radiopharmacy.

**Key Words:**  $^{90}\text{Y}$  radioembolization; selective internal radiation therapy;  $^{90}\text{Y}$  PET/CT; phantom; radiopharmacy

**J Nucl Med Technol 2014; 42:265–268**

DOI: 10.2967/jnmt.114.145292

---

**R**adioembolization of liver malignancies with  $^{90}\text{Y}$  is brachytherapy delivered by arterially injected  $\beta^-$ -emitting

microspheres, which may be made of resin (SIR-Spheres; Sirtex Medical Limited) or glass (TheraSphere; BTG). There has been recent interest in  $^{90}\text{Y}$  PET with concomitant low-dose CT. Coincidence imaging of  $^{90}\text{Y}$  is possible because of a minor decay branch to the  $0^+$  first excited state of  $^{90}\text{Zr}$ , followed by  $\beta^-\beta^+$  internal pair production, at a low branching ratio of  $31.86 \pm 0.47 \times 10^{-6}$  (1,2). Despite background noise in the reconstructed images due to naturally occurring  $^{176}\text{Lu}$  within the lutetium-based crystal of today's time-of-flight PET scanners, recent studies have shown  $^{90}\text{Y}$  PET quantification to be feasible and accurate (3–8).

For  $^{90}\text{Y}$  PET/CT phantom studies, homogeneous solutions of  $^{90}\text{Y}$ , for example,  $^{90}\text{Y}$ -citrate, are commonly used. However, the microsphere biodistribution of a postradioembolization liver is never homogeneous (9); therefore, such phantoms are physiologically unrealistic for simulating clinical scenarios. The aim of this work was to develop a safe and practical phantom capable of simulating the heterogeneous microsphere biodistribution of a postradioembolization liver throughout both tumor and nontumor liver compartments with a physiologically realistic tumor-to-normal liver ratio.

## MATERIALS AND METHODS

### Phantom Construction

Institutional Review Board approval was not required for the conduct and publication of this phantom study, which did not involve any human subjects. The phantom design was inspired by a gel-based phantom used by Goedicke et al. to overcome the problem of microsphere sedimentation (7). For this phantom, the medium used to suspend the microspheres was gelatin. A 5%-by-weight solution of gelatin was prepared by slowly dissolving 75 g of gelatin into 1,500 mL of distilled sterile water (for injection/irrigation). The solution was kept at 45°C on a hot plate and magnetically stirred at 300 rpm to ensure that the gelatin would not set. The liver phantom was a 1,330-mL rectangular homeware container made of clear, rigid plastic. The 2 tumor inserts were round containers made of similar plastic material, measuring 27 and 58 mL by volume. A magnetic stir bar (Spinbar; Sigma-Aldrich) was placed into each of the 3 inserts, and then the inserts were filled to maximum capacity with gelatin. The inserts were kept on a hot plate with the stir bar at 300 rpm to ensure proper distribution of heat and to prevent setting.

---

Received Jul. 3, 2014; revision accepted Oct. 15, 2014.

For correspondence or reprints contact: Yung Hsiang Kao, Department of Nuclear Medicine, Austin Hospital, Level 1, Harold Stokes Building, 145 Studley Rd., Heidelberg, Melbourne, Victoria 3084, Australia.

E-mail: yung.h.kao@gmail.com

Published online Nov. 11, 2014.

COPYRIGHT © 2014 by the Society of Nuclear Medicine and Molecular Imaging, Inc.

$^{90}\text{Y}$  resin microspheres from a full vial with a total activity of 3.144 GBq were carefully dispensed into each of the 3 inserts to achieve a realistic tumor-to-normal liver ratio of approximately 5 for hepatocellular carcinoma (10). The total vial activity was determined from calibration factors provided by the manufacturer, to an uncertainty of  $\pm 10\%$ . For this vial, the derived total activity of  $3.144 \pm 0.31$  GBq was in good agreement with the measured activity of 3.139 GBq by the dose calibrator (CRC-35; Capintec) using the  $^{90}\text{Y}$  setting of  $480 \times 10$ . Individual activities were  $281 \pm 28$  MBq in 27 mL (10.4 MBq/mL) and  $573 \pm 57$  MBq in 58 mL (9.9 MBq/mL) for the 2 tumor inserts and  $2,290 \pm 229$  MBq in 1,245 mL (1.8 MBq/mL) for the liver insert. All  $^{90}\text{Y}$  activities were determined by volume from the original vial of well-suspended microspheres. All microspheres were completely dispensed into the phantom, with negligible residual vial activity.

After the microspheres were added, the hot plate was turned off and the gelatin was rapidly cooled in an ice-water bath while still being stirred. This stirring process resulted in a gelatin-based suspension of heterogeneously distributed microspheres throughout both tumor and nontumor liver compartments. The magnetic stir bars were intentionally left within the inserts to simulate the metallic coils used for prophylactic coil embolization. The plastic lids of all 3 inserts were secured with adhesive tape. The 2 tumor inserts were placed into the liver insert to complete the liver phantom. Therefore, the whole-liver total activity was  $3.144 \pm 0.31$  GBq distributed throughout 1,330 mL of gelatin, with a mean radioconcentration of 2.36 MBq/mL. To simulate the attenuation within a patient, the liver phantom was fixed using adhesive strips near the bottom of a 5-liter plastic body phantom and further weighed down using saline bags placed on its lid. The body phantom was then completely filled with water and sealed with adhesive tape.

#### $^{90}\text{Y}$ PET/CT Protocol

$^{90}\text{Y}$  PET/CT scans were obtained on a Biograph mCT-S(64) 4R (Siemens Medical Solutions), which uses lutetium oxyorthosilicate crystals and has time-of-flight capability. Because  $^{90}\text{Y}$  was not available on this system as a radionuclide choice at the time of this study, all studies were acquired using  $^{86}\text{Y}$  settings, with a half-life of 14.74 h and a branching ratio of

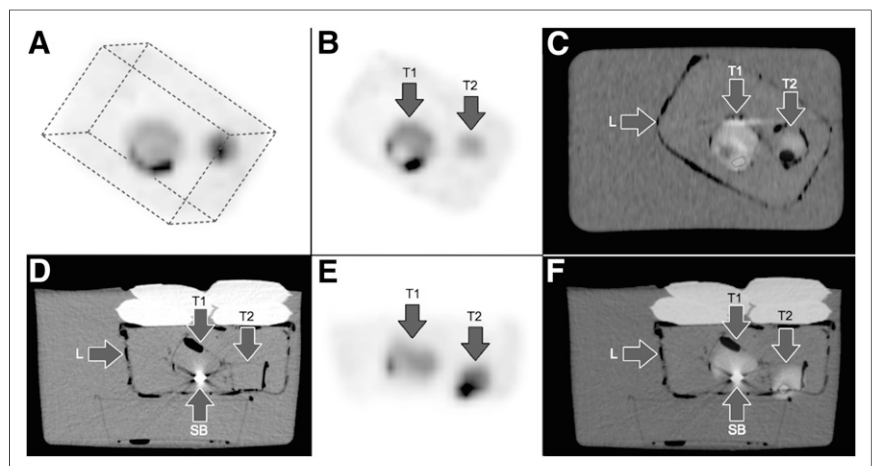
0.33. PET was acquired at 15 min per bed position and reconstructed using the vendor-supplied TrueX algorithm plus time-of-flight reconstruction (UltraHD-PET; Siemens) with 1 iteration, 21 subsets, and a filter of 8 mm, decay-corrected to the start of the scan. CT was performed at 120 kVp, 50 mAs (CARE Dose 4D; Siemens), a Z-coverage per rotation of  $64 \times 0.6$  mm, 5-mm slices, and a pitch of 0.75. All phantom scans were obtained using a single bed position. All reconstructed  $^{90}\text{Y}$  PET/CT images were qualitatively reviewed;  $^{90}\text{Y}$  PET quantification of activity was not performed.

#### Phantom Physical Density

The main constituent of gelatin is collagen. Because our liver phantom was prepared in a nonsterile manner, environmental bacteria or fungi may have been inadvertently introduced into the phantom, with the potential to cause gelatin hydrolysis. Furthermore, the effect of  $^{90}\text{Y}$   $\beta$  radiation on the structural integrity of gelatin has not been well described. For our study, the physical density ( $\text{g}/\text{cm}^3$ ) of the liver phantom was empirically used as a surrogate measure of possible gelatin breakdown or leakage occurring during the study. We postulated that as gelatin degrades, its density may change due to the upward migration of air pockets trapped during preparation of the liver phantom.

To avoid radiation exposure to the operator, the physical density of gelatin was indirectly measured based on the CT component of the PET/CT scan. By assuming a linear relationship between the CT number (Hounsfield unit) and the physical density of a water-based object of interest (11), we calculated the physical density of the liver phantom as  $(\text{mean CT number} + 1,000)/1,000$ . CT analysis was performed using OsiriX software (version 5.6; Pixmeo). The mean CT number of the liver phantom was determined from a cylindrical volume of interest with a 4-cm diameter and 4.5-cm length, placed within a region of gelatin free from large air pockets or tumor inserts. This volume of interest was repeated across all phantom scans to obtain its mean physical density and compared with an expected result of  $1.05 \text{ g}/\text{cm}^3$ . As a control, the physical density of water within the body phantom was similarly measured and compared with an expected result of  $1 \text{ g}/\text{cm}^3$ .

**FIGURE 1.** Gelatin-based liver phantom containing suspended  $^{90}\text{Y}$  resin microspheres. (A) Maximum-intensity projection of liver phantom in oblique view. Dotted lines outline liver phantom. (B and C)  $^{90}\text{Y}$  PET/CT scan in coronal plane demonstrates heterogeneous distribution of  $^{90}\text{Y}$  resin microspheres within 2 tumor inserts, T1 and T2, and throughout nontumorous liver, L. Small air pockets can be seen within and around tumor inserts and liver phantom. (D–F)  $^{90}\text{Y}$  PET/CT in transaxial view demonstrates CT artifacts caused by a magnetic stir-bar (SB) at bottom of T1 tumor insert. (A color version of this figure is available as a supplemental file online at <http://tech.snmjournals.org/>.)



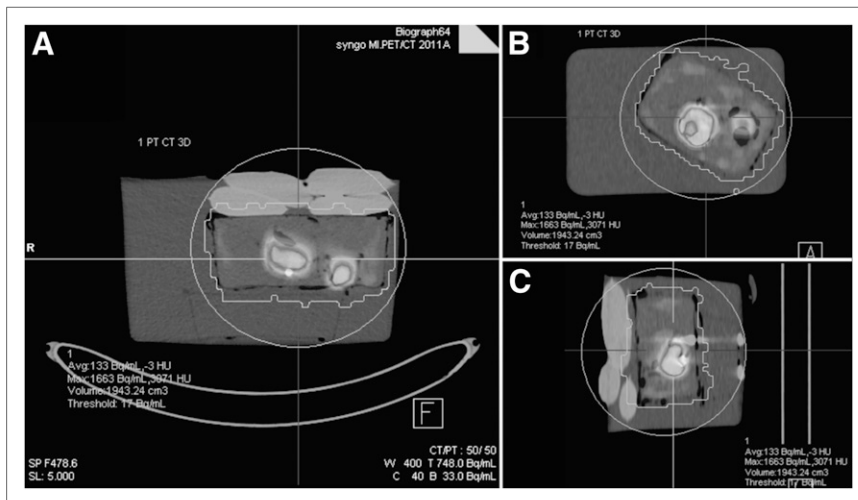


**FIGURE 2.** Example of volume-of-interest analysis of  $^{90}\text{Y}$  PET/CT phantom scan generated using 1% volumetric isocontour threshold, which may be used for quantitative analysis. Images are shown in transaxial (A), coronal (B), and sagittal planes (C). (A color version of this figure is available as a supplemental file online at <http://tech.snmjournals.org/>.)

## RESULTS

Twelve phantom scans were acquired over 13 d. All scans demonstrated a heterogeneous distribution of  $^{90}\text{Y}$  microspheres throughout the liver and tumor inserts, fixed and suspended within the gelatin (Fig. 1). Barring the expected deterioration in perceived image quality due to increasing noise as  $^{90}\text{Y}$  decayed over the course of the study, the overall visual activity distribution within the phantom was generally unchanged.

Serendipitously, magnetic stir bars left inside the liver phantom produced CT artifacts similar to those caused by embolization coils, and pockets of air trapped inside the gelatin during its preparation mimicked gas within hollow viscus. Throughout the study, the 2 tumor inserts remained unchanged in position and there was no detectable activity along the bottom of the water-filled body phantom to suggest any sedimentation of leaked  $^{90}\text{Y}$  resin microspheres.

The physical density of the liver phantom was estimated as  $1.011 \pm 0.0012 \text{ g/cm}^3$  (median,  $1.011 \text{ g/cm}^3$ ; 95% confidence interval, 1.010–1.011), which remained unchanged throughout the study, and was lower than the expected density of  $1.05 \text{ g/cm}^3$ , likely due to pockets of air trapped within the gelatin. As a methodologic control, the physical density of water in the body phantom was estimated as  $1.0017 \pm 0.00066 \text{ g/cm}^3$  (median,  $1.0017 \text{ g/cm}^3$ ; 95% confidence interval, 1.0013–1.0021), representing a low mean error of less than 0.2%, and provided quality assurance for this technique.

## DISCUSSION

Although homogeneous solutions of  $^{90}\text{Y}$  (e.g.,  $^{90}\text{Y}$ -citrate) are less affected by uncertainties in activity measurement and are convenient for use in phantom studies, they do not represent the physiologic reality of a postradioembolization liver. This study has achieved its objective of developing a phantom capable of simulating the heterogeneous distribution of microspheres in both tumor and nontumor liver com-

partments, with a realistic tumor-to-normal liver ratio. Such a phantom may have theoretic benefits in improving the qualitative and quantitative accuracy of  $^{90}\text{Y}$  PET/CT phantom scans when simulating postradioembolization clinical scenarios (Fig. 2).

For this phantom design, the tumor inserts and  $^{90}\text{Y}$  resin microspheres remained fixed and suspended within the gelatin throughout a 2-wk period, with no evidence of breakdown or microsphere leakage. This phantom was made from materials readily available in a radiopharmacy and was feasible to construct.

There were several limitations to this study. First,  $^{90}\text{Y}$  PET activity quantification or voxel-based analyses were not adequately performed at the time of this report because technical issues related to our scan protocols were still being optimized. Second, our phantom was not anthropometrically realistic of the liver and abdomen and was also missing the lungs and skeleton. The impact of such anatomic discrepancies was not investigated in this study. Third, although we achieved a realistic tumor-to-normal liver ratio of approximately 5 for hepatocellular carcinoma, the heterogeneous distribution of microspheres would not be exactly reproducible at the microscopic level from phantom to phantom, which is an inherent limitation of our phantom construction technique. Last, although the magnetic spin bars left intentionally within the liver phantom produced CT artifacts visually similar to those of embolization coils, the physical shape and metallic composition of the spin bars (alloy of aluminum, nickel, iron, and cobalt) were different from those of embolization coils (platinum-based). The effects of these physical differences were not further investigated.

## CONCLUSION

A gelatin-based liver phantom realistically simulating the physiologic biodistribution of  $^{90}\text{Y}$  resin microspheres in a postradioembolization liver is safe and feasible.

## DISCLOSURE

No potential conflict of interest relevant to this article was reported.

## REFERENCES

1. Kao YH, Steinberg JD, Tay YS, et al. Post-radioembolization yttrium-90 PET/CT: part 2—dose-response and tumor predictive dosimetry for resin microspheres. *EJNMMI Res.* 2013;3:57.
2. Selwyn RG, Nickles RJ, Thomadsen BR, DeWerd LA, Micka JA. A new internal pair production branching ratio of  $^{90}\text{Y}$ : the development of a non-destructive assay for  $^{90}\text{Y}$  and  $^{90}\text{Sr}$ . *Appl Radiat Isot.* 2007;65:318–327.
3. Lhommel R, van Elmbt L, Goffette P, et al. Feasibility of  $^{90}\text{Y}$  TOF PET-based dosimetry in liver metastasis therapy using SIR-Spheres. *Eur J Nucl Med Mol Imaging.* 2010;37:1654–1662.
4. Walrand S, Flux GD, Konijnenberg MW, et al. Dosimetry of yttrium-labelled radiopharmaceuticals for internal therapy:  $^{86}\text{Y}$  or  $^{90}\text{Y}$  imaging? *Eur J Nucl Med Mol Imaging.* 2011;38(suppl 1):S57–S68.
5. Walrand S, Lhommel R, Goffette P, Van den Eynde M, Pauwels S, Jamar F. Hemoglobin level significantly impacts the tumor cell survival fraction in humans after internal radiotherapy. *EJNMMI Res.* 2012;2:20.
6. Willowson K, Forwood N, Jakoby BW, Smith AM, Bailey DL. Quantitative  $^{90}\text{Y}$  image reconstruction in PET. *Med Phys.* 2012;39:7153–7159.
7. Goedicke A, Berker Y, Verburg F, Behrendt F, Winz O, Mottaghy F. Study-parameter impact in quantitative 90-yttrium PET imaging for radioembolization treatment monitoring and dosimetry. *IEEE Trans Med Imaging.* 2013;32:485–492.
8. Elschot M, Vermolen BJ, Lam MG, de Keizer B, van den Bosch MA, de Jong HW. Quantitative comparison of PET and Bremsstrahlung SPECT for imaging the in vivo yttrium-90 microsphere distribution after liver radioembolization. *PLoS ONE.* 2013;8:e55742.
9. Kennedy AS, Nutting C, Coldwell D, Gaiser J, Drachenberg C. Pathologic response and microdosimetry of  $^{90}\text{Y}$  microspheres in man: review of four explanted whole livers. *Int J Radiat Oncol Biol Phys.* 2004;60:1552–1563.
10. Kao YH, Tan EH, Burgmans MC, et al. Image-guided personalized predictive dosimetry by artery-specific SPECT/CT partition modeling for safe and effective  $^{90}\text{Y}$  radioembolization. *J Nucl Med.* 2012;53:559–566.
11. Mull RT. Mass estimates by computed tomography: physical density from CT numbers. *AJR.* 1984;143:1101–1104.